

High-resolution powder diffraction study of purple membrane with a large Guinier-type camera

Toshihiko Oka,^{a,b*} Keiko Miura,^b Katsuaki Inoue,^b Tatzuo Ueki^b and Naoto Yagi^b

Received 15 November 2005

Accepted 8 February 2006

^aDepartment of Physics, Faculty of Science and Technology, Keio University, Japan, and ^bResearch and Utilization Division, SPring-8/JASRI, Japan. E-mail: oka@phys.keio.ac.jp

X-ray diffraction patterns from a film of oriented purple membranes, which comprise two-dimensional crystals of bacteriorhodopsin (BR) trimers, were recorded with a 1 m-pathlength Guinier-type camera at SPring-8 BL40B2. A well focused X-ray beam and a camera with a high angular resolution of 0.024° enabled a powder diffraction profile with very sharp and well separated peaks to be obtained up to a resolution of 2.3 \AA . Using integrated diffraction intensities up to a Bragg spacing of 4.2 \AA , a cluster of bulky amino acid residues and the head group of the BR chromophore are apparent in the electron density map projected along the membrane normal. Thus, a combination of synchrotron X-rays and large Guinier camera can be used for analyzing the conformational changes of BR in the intact state. In addition, the method might be extended to the structural analysis of film materials composed of two-dimensional arrays of nanoparticles.

© 2006 International Union of Crystallography
Printed in Great Britain – all rights reserved**Keywords:** bacteriorhodopsin; powder diffraction; SPring-8.

1. Introduction

In recent years, X-ray crystallography has provided three-dimensional structures of membrane proteins and components of filamentous assemblies of proteins (Toyoshima *et al.*, 2000; Ferreira *et al.*, 2004; Samatey *et al.*, 2004). To further understand the actions of those proteins in living cells, their structures and dynamics must be studied in their natural environment. X-ray diffraction can be used to study biological membranes and filamentous materials under physiological conditions. In the early stage of structural biology about 30 years ago, some studies revealed low-resolution structures of the supramolecular assemblies of proteins in biological membranes (Blaurock, 1975; Ueki *et al.*, 1976; Makowski *et al.*, 1977). In addition, X-ray diffraction studies on oriented sols of filamentous materials such as tobacco mosaic virus (Namba *et al.*, 1989), actin filament (Holmes *et al.*, 1990; Oda *et al.*, 1998) and bacterial flagella (Yamashita *et al.*, 1998) have provided important structural information on the inter-subunit interactions driving the self-assemblies of the proteins in their intact environment, despite many difficulties in the diffraction experiments.

Acquiring high-resolution diffraction data of the samples of protein assemblies requires a small X-ray beam and a detector system with a high spatial resolution and a wide dynamic range. X-ray beams provided from the third-generation synchrotron facilities have small diameters and low angular divergences. Imaging-plate (IP) detectors with a spatial resolution of about $100 \mu\text{m}$ and a dynamic range of 10^5 are suitable for recording their diffraction patterns, because stacked biological membranes and oriented sols of filamentous assemblies of proteins have long-ordered structures and display wide-ranging intensity resolutions.

We have developed a Guinier camera for powder diffraction experiments of microcrystalline materials with large unit cells (Miura

et al., 2004). The camera has a maximum specimen-to-detector distance of 1000 mm, and its maximum angular resolution is 0.024° with a blue IP of spatial resolution $100 \mu\text{m}$ (Amemiya, 1995; Yamamoto *et al.*, 1998). The high angular resolution is suitable for X-ray diffraction experiments of biological membranes and sols of filamentous biological materials because diffraction peaks of the samples at high angles are close to each other and inseparable with low-resolution detectors.

Powder X-ray diffraction experiments for biological materials are applied in structural studies on purple membrane (PM), which is a two-dimensional crystalline array of bacteriorhodopsin (BR) acting as a light-driven proton pump on the cell membrane of *Halo-bacterium salinarium* (Haupts *et al.*, 1999). An orientated PM sample diffracts X-rays up to a resolution of 4 \AA with a laboratory source (Henderson, 1975); however, it is difficult to separate the diffraction peaks and to evaluate diffraction intensities beyond a resolution of 7.0 \AA because of beam divergence and the low angular resolution of the detector system. Thus, X-ray diffraction studies of PM on the structural changes during proton pumping have been limited to low resolution even in recent years (Nakasako *et al.*, 1991; Koch *et al.*, 1991; Oka *et al.*, 2000, 2002, 2005). To date, X-ray crystal structure analysis has revealed structural changes in proton pumping for some crystal forms of BR with different molecular packing from PM (for reviews, see Lanyi & Schobert, 2004; Hirai & Subramania, 2003). In those crystals, BR molecules are arranged into a molecular packing that is different from that in PM, and have extra interactions which are absent in PM. Thus, it is difficult to deny the possibility that the interactions alter the intact photoreaction and accompanying structural change. In fact, recent studies propose different modes of structural change (Lanyi & Schobert, 2003; Lanyi, 2004; Kouyama *et al.*, 2004). To understand the effects of molecular packing on proton pumping and to elucidate the dynamics of BR in living cells, X-ray

diffraction experiments on intact PM film or ultimately on a single PM are necessary.

In our first attempt to use the Guinier camera for structural studies of biological macromolecular assemblies, we carried out X-ray diffraction experiments on oriented films of PMs with the Guinier camera and quantitatively evaluated the feasibility of the systems for visualizing conformational changes of BR at work. The angular resolution of the camera system in combination with the X-ray beam provided by a bending magnet of SPring-8 enabled us to record the diffraction patterns of PM films up to a spacing of 2.3 Å. A projected density map calculated using the diffraction data at a resolution of 4.2 Å displayed the characteristics expected from a crystal structure of BR.

2. Methods

2.1. Sample preparation

The PM of BR isolated from *H. salinarium* through a conventional procedure (Oesterhelt & Stoerkenius, 1974) was concentrated in a buffer containing 10 mM (pH 7.0) MOPS (3-morpholinopropane-sulfonic acid) so that the absorbance of the solution was 20 at 570 nm. A film of PM was made by applying a 45 µl solution to a quartz plate of thickness 20 µm and letting it dry to build up a sufficiently thick sample film. This procedure made a plane of PM parallel to that of a quartz plate. Then the plate was cut into a rectangular shape, about 1 mm × 5 mm. The sample plate was glued to a thin glass fiber, and the relative humidity of the sample was kept at 75% by using saturated NaCl solution (O'Brien, 1948) for about 1 day. There are approximately 4×10^4 PM layers in the sample, and a single PM is approximately 5 nm thick.

2.2. X-ray diffraction experiment

The X-ray diffraction experiments were carried out at BL40B2 of SPring-8 (Inoue *et al.*, 2004). A powder diffractometer of the Guinier geometry (Miura *et al.*, 2004) was used to record diffraction patterns. The maximum specimen-to-detector length of the diffractometer was set to 1000 mm. The X-rays, whose wavelengths were tuned to 1.000 Å, were focused with a cylindrical mirror so that the cross section was 0.25 mm (horizontal) × 0.20 mm (vertical) at the detector position, and the flux density of the focused X-ray beam was 2×10^{12} photons s⁻¹ mm⁻². The PM sample was flash-cooled and kept at 110 K by a N₂ gas stream from a cooling device (Rigaku, Japan) to suppress radiation damage. The plane of the film sample was set to be parallel to the incident X-ray beam so that the X-ray grazed the film surface with grazing-incidence geometry. Diffraction patterns were recorded with a 200 mm × 400 mm blue IP (BAS-SR2040, Fujifilm, Japan), which was scanned at a resolution of 50 µm with a BAS2500 IP reader (Fujifilm, Japan). Because the size of the IP was too short to record whole diffraction patterns of the sample from low to high angle (corresponding to a 2θ value from 0° to 30°) regions at once, two diffraction patterns were recorded separately at a low-to-middle region (from 0° to 17°) and another at a middle-to-high angle (from 9° to 30°). The exposure time of each image was 30 min. Scattering patterns from a quartz plate were also recorded at the two regions to subtract the background.

2.3. Data analysis

One-dimensional diffraction profiles were calculated by circularly averaging 20° sectors on the low-to-middle and middle-to-high angle images across the equatorial direction (Fig. 1). After subtracting the

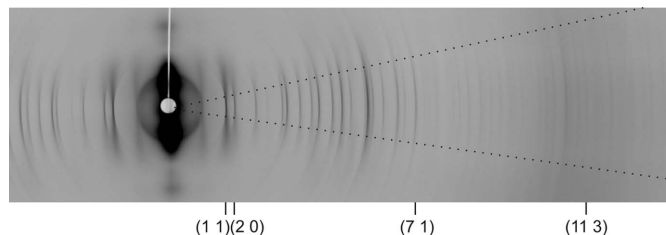


Figure 1

An X-ray diffraction pattern of a PM film recorded on an IP with the Guinier camera. PM is a well ordered two-dimensional crystal of BR trimers arranged in a hexagonal lattice belonging to plane group *p3*. The right-hand edge of the image corresponds to a resolution of 3.5 Å. The plane of the film is parallel to the incident X-ray, and the normal of the film is parallel to the vertical of the image. The arc across the equatorial line indicates the imperfect orientations of PMs in the film sample. Along the meridional axis, strong lamellar diffraction peaks coming from the layers of PM are seen. Miller indices of some reflections [(1 1), (2 0), (7 1) and (11 3)] are indicated. The (7 1) and (11 3) reflections correspond to a spacing of 7.0 Å and 4.2 Å. Dotted lines indicate edges of the sector within which a one-dimensional diffraction profile was circularly integrated and averaged (see Fig. 2). The central angle of the sector is 20°.

background scattering from a quartz plate, the diffraction patterns recorded in the low-to-middle and middle-to-high angle regions were merged by multiplying by a scale factor. The integrated 52 intensities of Bragg reflections up to 4.2 Å were calculated using a least-squares fitting method with a Gauss function convolved with an exponential function (Nakasako *et al.*, 1991).

Because Bragg reflections of different indices with the same Bragg spacing overlapped in many diffraction peaks, the diffraction intensities of individual reflections were calculated by using the ratio of the amplitude obtained from cryoelectron microscopy for single PMs (Henderson *et al.*, 1990). Fourier electron density maps projected along the normal of the membrane plane were calculated using a phase set reported in the cryoelectron microscopic study of PM (Henderson *et al.*, 1990). Calculations were carried out using *Igor Pro 4* (Wavemetrics, USA).

3. Results

The diffraction power of a single PM is very weak because it is only about 0.5 µm across. However, the sample of this study, containing many oriented PMs, can diffract X-rays to a high resolution. Fig. 1 shows a typical diffraction pattern of the sample at the low-to-middle angle region up to a diffraction angle of 17°. The diffraction pattern comprises a series of arcs extending to meridional directions from the equator. Although strong diffraction arcs are observed up to the (7 1) reflection, a Bragg spacing of 7.0 Å, weak but clear arcs are visible to the edge of the IP, corresponding to a spacing of 3.5 Å. In the diffraction pattern in the middle-to-high angle region up to 30° (a resolution of 2.0 Å), diffraction arcs are still apparent up to a resolution of 2.3 Å (pattern not shown). Thus, the combination of a small X-ray beam and the Guinier camera enabled the diffraction pattern of a PM film to be recorded at the highest ever resolution. The X-ray exposure is 30 min, but intensity change or position movement is not observed by keeping the sample at 110 K.

Fig. 2 shows a one-dimensional diffraction profile of the PM film reduced from the diffraction patterns from the low-to-middle angle image in Fig. 1 and a middle-to-high angle. The simple scaling procedure for merging the two diffraction patterns in different angular regions works well. Intensities of diffraction peaks decrease gradually with an increase in scattering vector *S*, but peaks are visible beyond 0.40 Å⁻¹ (2.5 Å resolution). The lattice constant of PM at around 110 K was calculated to be 61.03 ± 0.10 Å from the positions

of 47 sharp diffraction peaks located between 0.03 and 0.32 \AA^{-1} . The expected positions of diffraction peaks from a hexagonal lattice correspond exactly to the observed peak positions in the diffraction profile (Fig. 2). As a result, 52 diffraction intensities of 55 expected reflections from (1 0) to (11 3) are integrated using the profile-fitting method.

An electron density map of BR projected normal to the membrane plane was calculated at a resolution of 4.2 \AA (Fig. 3). The map clearly indicates the electron density of seven transmembrane α -helices and its trimer structure. When the map is compared with those in previous studies obtained at a resolution of 7 \AA (Nakasako *et al.*, 1991; Oka *et al.*, 1999, 2000), it displays characteristics that were observed in a projection map calculated at a resolution of around 3.5 \AA by electron microscopy (Henderson *et al.*, 1986). Firstly, the four helices (A, E, F and G) located at the outer rim of the BR monomer have projection densities lower than the three helices (B, C and D) in the inner part. This characteristic comes from the tilting of the four helices from the

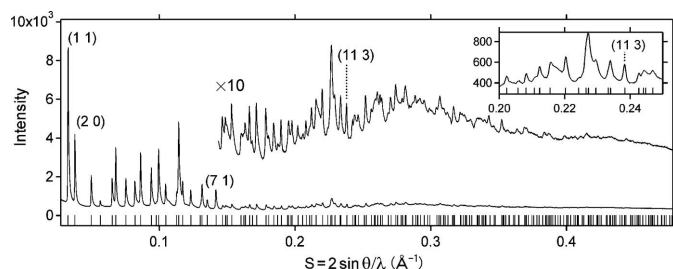


Figure 2

An X-ray diffraction profile of PM merged from two circularly averaged diffraction profiles recorded in the low-to-middle angle (from 0° to 17°) (Fig. 1) and middle-to-high angle (from 9° to 30°) regions. The diffraction profile beyond 0.144 \AA^{-1} , magnified in the intensity scale, is also shown. The diffraction peaks are visible up to 0.44 \AA^{-1} (a resolution of 2.3 \AA). Bars below the diffraction profile are expected positions of diffraction peaks from a hexagonal lattice of plane group $p3$. The inset shows the magnified profile between 0.20 and 0.25 \AA^{-1} to demonstrate the angular resolution of the system to separate diffraction peaks. Miller indices of reflections (1 1), (2 0), (7 1) and (11 3) shown in Fig. 1 are also depicted. The lattice constant of PM at around 110 K was calculated to be $61.03 \pm 0.10 \text{ \AA}$.

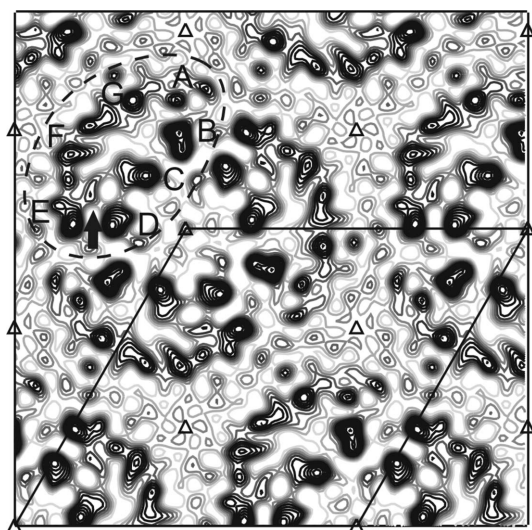


Figure 3

Electron density map of PM projected onto a membrane plane. It was calculated with the diffraction amplitudes up to the (11 3) reflection, a resolution of 4.2 \AA . The envelope shown by the dashed line shows the border of one BR monomer, and the characters A–G are the names of seven transmembrane α -helices. The triangle symbols denote the positions of threefold-rotational symmetry points. The arrow indicates a density peak that appears in the region surrounded by helices C, D, E and F (see results).

membrane normal as demonstrated in the crystal structure of BR (Leucke *et al.*, 1999). Secondly, small but significant density peaks are visible in the map. In particular, a small peak is identified between helices C, D, E and F. Such a peak is invisible in the maps at 7 \AA . When referring to the crystal structure (Leucke *et al.*, 1999), the small peak plausibly corresponds to the electron densities of the β -ionone group of the chromophore retinal and the side chain of Trp189 adjoining the chromophore.

4. Discussion

In powder diffraction studies, as the diffraction angle becomes larger the number of peaks increases and the peaks become wider and weaker. As a result it is difficult to distinguish each diffraction peak separately at a high diffraction angle (Nakasako *et al.*, 1991; Oka *et al.*, 1999, 2000). Using a flat IP detector with 50 cm camera length, Bragg peaks were observed up to around 2.5 \AA , but the intensities were evaluated with the profile-fitting method only to a resolution of 5.3 \AA (unpublished result). In contrast, owing to the high angular resolution of the large Guinier camera, observed peaks became sharp up to a high resolution (Fig. 2) and peak widths became narrower than half of that of the unpublished results. As a result, intensities were evaluated up to a spacing of 4.2 \AA . The present experimental data for PMs suggest the possibility of X-ray diffraction experiments for structural studies of intact biological membranes and macromolecule assemblies. In particular, the camera seems to be advantageous for studying powder diffraction of three-dimensional crystals of protein (Von Dreele *et al.*, 2000). The number of diffraction peaks of a three-dimensional crystal is larger than that of a two-dimensional crystal with the same lattice constant. Therefore, high spatial resolution of the camera would increase the number of observable peaks and improve data quality in the powder diffraction study of three-dimensional crystals.

The present study demonstrates the feasibility of the Guinier camera in collecting diffraction data of biological membranes. The camera enables the quantitative evaluation of the diffraction intensities up to the (11 3) reflection with the profile-fitting method. However, overlaps, weak intensities and spread of peak width make it difficult to evaluate diffraction intensities at higher resolution. Therefore, two techniques must be incorporated in the experiments to improve the fitting methods. One is the utilization of undulator X-rays. In this experiment we used X-rays from a bending magnet. The full width of the vertical beam size that affects the resolution of the camera is about 200 \mu m , which is four times larger than the pixel size of the detector. On the contrary, the undulator X-rays are easily focused to a vertical beam size of less than 50 \mu m with a mirror. A highly focused intense X-ray beam improves the overlaps of diffraction peaks and lowers the statistical errors of intensities. The other technique is the improvement in sample preparation. The PM in the present experiment is not highly oriented. For instance, ultracentrifugation was used to improve the orientation of PM (Henderson, 1975). Moreover, by applying a high magnetic field to the sample area, the orientation of biological nanoparticles may become better and suppress the spread of diffraction intensities (Glucksman *et al.*, 1986; Oda *et al.*, 1998).

In the present study we used PM as a sample. Now, the structural studies of BR focus on the conformational changes in proton pumping during the photoreaction cycle of the protein. Some crystal structure analyses of reaction intermediates have been reported using different crystal systems; there is, however, controversy regarding the structural changes (Lanyi & Schobert, 2003; Lanyi, 2004; Kouyama *et*

al., 2004). Molecular contacts formed in the crystallization process may affect the conformational changes. When evaluating the statistics of the present experimental system for PM, intensity changes of less than 1% in reflections around the (11 3) peak may be detectable. Therefore, structural studies of the reaction intermediates in the intact state will be possible and may provide clues to understanding the conformational changes and mechanism in proton pumping of BR.

We are grateful to Professor M. Nakasako for critical reading of the manuscript. The synchrotron radiation experiments were performed at SPring-8 with the approval of the Program Review Committee of the Japan Synchrotron Radiation Research Institute (JASRI) (proposals nos. 2003A0173-NL2-np, 2003B0270-NL2a-np and 2004A0304-CL2a-np). This research was partially supported by the Ministry of Education, Science, Sports and Culture, Grants-in-Aids 14780519, 15076210 and 17770131 to TO.

References

- Amemiya, Y. (1995). *J. Synchrotron Rad.* **2**, 13–21.
- Blaurock, A. E. (1975). *J. Mol. Biol.* **93**, 139–158.
- Ferreira, K. N., Iverson, T. M., Maghlaoui, K., Barber, J. & Iwata, S. (2004). *Science*, **303**, 1831–1838.
- Glucksman, M. J., Hay, R. D. & Makowski, L. (1986). *Science*, **231**, 1273–1276.
- Haupts, U., Tittor, J. & Oesterhelt, D. (1999). *Annu. Rev. Biophys. Biomol. Struct.* **28**, 367–399.
- Henderson, R. (1975). *J. Mol. Biol.* **93**, 123–138.
- Henderson, R., Baldwin, J., Ceska, T. A., Zemlin, F., Beckmann, E. & Downing, K. H. (1990). *J. Mol. Biol.* **213**, 899–929.
- Henderson, R., Baldwin, K. H., Downing, J., Lepault, J. & Zemlin, F. (1986). *Ultramicroscopy*, **19**, 147–178.
- Hiari, T. & Subramaniam, S. (2003). *FEBS Lett.* **545**, 2–8.
- Holmes, K. C., Popp, D., Gebhard, W. & Kabsch, W. (1990). *Nature (London)*, **347**, 44–49.
- Inoue, K., Oka, T., Miura, K. & Yagi, N. (2004). *AIP Conf. Proc.* **705**, 336–339.
- Koch, M. H., Dencher, N. A., Oesterhelt, D., Plohn, H. J., Rapp, G. & Buldt, G. (1991). *EMBO J.* **10**, 521–526.
- Kouyama, T., Nishikawa, T., Tokuhisa, T. & Okumura, H. (2004). *J. Mol. Biol.* **335**, 531–546.
- Lanyi, J. K. (2004). *Biochim. Biophys. Acta*, **1658**, 14–22.
- Lanyi, J. K. & Schobert, B. (2003). *J. Mol. Biol.* **328**, 439–450.
- Lanyi, J. K. & Schobert, B. (2004). *Biochemistry*, **42**, 3–8.
- Leucke, H., Schobert, B., Richter, H.-T., Cartailler, J.-P. & Lanyi, J. K. (1999). *J. Mol. Biol.* **291**, 899–911.
- Makowski, L., Caspar, D. L. D., Phillips, W. C. & Goodenough, D. A. (1977). *J. Cell Biol.* **74**, 629–645.
- Miura, K., Inoue, K., Goto, S., Ishikawa, T., Yamamoto, M. & Ueki, T. (2004). *AIP Conf. Proc.* **705**, 989–902.
- Nakasako, M., Kataoka, M., Amemiya, Y. & Tokunaga, F. (1991). *FEBS Lett.* **292**, 73–75.
- Namba, K., Pattanayek, R. & Stubbs, G. (1989). *J. Mol. Biol.* **208**, 307–325.
- O'Brien, F. E. M. (1948). *J. Sci. Instrum.* **25**, 73–76.
- Oda, T., Makino, K., Yamashita, I., Namba, K. & Maeda, Y. (1998). *Biophys. J.* **75**, 2672–2681.
- Oesterhelt, D. & Stoeckenius, W. (1974). *Methods Enzymol.* **31**, 667–678.
- Oka, T., Inoue, K., Kataoka, M. & Yagi, N. (2005). *Biophys. J.* **88**, 436–442.
- Oka, T., Kamikubo, H., Tokunaga, F., Lanyi, J. K., Needleman, R. & Kataoka, M. (1999). *Biophys. J.* **76**, 1018–1023.
- Oka, T., Yagi, N., Fujisawa, T., Kamikubo, H., Tokunaga, F. & Kataoka, M. (2000). *Proc. Natl. Acad. Sci. USA*, **97**, 14278–14282.
- Oka, T., Yagi, N., Tokunaga, F. & Kataoka, M. (2002). *Biophys. J.* **82**, 2610–2616.
- Samatey, F. A., Matsunami, H., Imada, K., Nagashima, S., Shaikh, T. R., Thomas, D. R., Chen, J. Z., Derosier, D. J., Kitao, A. & Namba, K. (2004). *Nature (London)*, **431**, 1062–1068.
- Toyoshima, C., Nakasako, M., Nomura, H. & Ogawa, H. (2000). *Nature (London)*, **405**, 647–655.
- Ueki, T., Kataoka, M. & Mitsui, T. (1976). *Nature (London)*, **262**, 809–810.
- Von Dreele, R. B., Stephens, P. W., Smith, G. D. & Blessing, R. H. (2000). *Acta Cryst. D* **56**, 1549–1553.
- Yamamoto, M., Kumasaka, T., Uruga, T., Kamiya, N., Iwasaki, H. & Ueki, T. (1998). *Nucl. Instrum. Methods*, **A416**, 314–318.
- Yamashita, I., Hasegawa, K., Suzuki, H., Vondervistzt, F., Mimori-Kiyosue, Y. & Namba, K. (1998). *Nature Struct. Biol.* **5**, 125–132.